Millennial changes in North American wildfire and soil activity over the last glacial cycle

Hubertus Fischer[1*], Simon Schüpbach[1], Gideon Gfeller[1], Matthias Bigler[1], Regine Röthlisberger[1], Tobias Erhardt[1], Thomas F. Stocker[1], Robert Mulvaney[2], Eric W. Wolff[3]

[1] Climate and Environmental Physics, Physics Institute & Oeschger Centre for Climate Change Research, University of Bern, Sidlerstrasse 5, 3012 Bern, Switzerland, hubertus.fischer@climate.unibe.ch

[2] British Antarctic Survey, Cambridge, U.K.

[3] Department of Earth Sciences, University of Cambridge, Cambridge, U.K.

Climate changes in the North Atlantic region during the last glacial cycle were dominated by the slow waxing and waning of the North American ice sheet as well as by intermittent Dansgaard-Oeschger (DO) events. However prior to the last deglaciation, little is known about the response of North American vegetation to such rapid climate changes and especially about the response of biomass burning, an important factor for regional changes in radiative forcing. Here we use continuous, high-resolution ammonium (NH_4^+) records derived from the NGRIP and GRIP ice cores to document both North American NH_4^+ background emissions from soils and wildfire frequency over the last 110,000 yr. Soil emissions increased on orbital timescales with warmer climate, related to the northward expansion of vegetation due to reduced ice-covered areas. During Marine Isotope Stage (MIS) 3 DO warm events, a higher fire recurrence rate is recorded, while

NH_4^+ soil emissions rose only slowly during longer interstadial warm periods, in line with slow ice sheet shrinkage and delayed ecosystem changes. Our results indicate that sudden warming events had little impact on NH_4^+ soil emissions and NH_4^+ aerosol transport to Greenland during the glacial but triggered a significant increase in the frequency of fire occurrence.

Wildfires represent an important driver in ecosystem development[1] and pyrogenic emissions of trace gases, black carbon and other aerosol components have a strong regional effect on the radiation balance and atmospheric chemistry[2]. A detailed understanding of the response of vegetation and wildfire activity to climate change is hampered by the relatively long timescales of ecosystem change and fire recurrence. Paleoclimate information can help in this regard, documenting a wide range of climate and environmental changes on orbital, millennial and decadal timescales.

During the last glacial cycle, the climate of the northern hemisphere was fundamentally altered as ice cover and sea level varied[3], impacting the areal extent of vegetation and its composition. On top of these slow changes, the North Atlantic region was characterized by rapid DO warmings, where temperatures in Greenland increased by 10-15°C in a few decades[4,5]. These events also had strong, far-field effects on boreal and tropical methane emissions[6], monsoon intensity[7] and dust emissions in Chinese desert areas[8,9]. However, there is little paleoclimate information available from North America (NA), especially at a resolution allowing the identification of DO events in continental, ice-free regions[10-14]. In particular, the continent-wide reconstruction of wildfire activity based on charcoal records does not extend beyond the last glacial/interglacial transition[1,15].

North American soil and wildfire signal in Greenland ice cores

Greenland ice cores can fill this gap because aerosol-transported NH_4^+ in the ice comes from NA soil emissions but (together with other pyrogenic aerosol tracers[16,17]) also from NA wildfire events[17,18]. Background NH_4^+ concentrations in Greenland are derived mainly from bacterial decomposition of nitrogen in NA soils[19], leading to a broad NH_4^+ summer maximum in Greenland ice[18,20]. On top of this mean annual cycle, very large peaks are detected during individual summers, caused by NA biomass burning events[21,22], also characterised by co-occurring peaks in fire-specific organic aerosol compounds[17,23]. These events exceed the NH_4^+ background by more than an order of magnitude and dominate the Greenland NH_4^+ budget in those years[18,20]. The imprint of these events is strongly dependent on atmospheric circulation at the time of the fire, which must be favourable for long-range transport from NA to Greenland. Accordingly, not all fire events are recorded in Greenland ice. However, averaged over a sufficient time period, ice core records can provide a reliable picture of relative changes in NA wildfire frequency[18]. When measured at high resolution, the NH_4^+ ice core record can provide the change in average background NH_4^+ from soil emissions, concentrations of fire events above this background and fire peak frequency (FPF).

In this study, Greenland NH_4^+ concentrations were measured in cm-resolution on the NGRIP ice core with our Continuous Flow Analysis[24,25] system and complemented by published data from the GRIP[18] ice core. The changes in these ice cores show essentially the same variations on millennial down to decadal timescales (Figures 2-4), proving that our records provide a reliable picture of NH_4^+ deposition in Greenland. Here we concentrate on the higher resolution NGRIP record, providing a continuous record from

10,000-110,000 yr before present (BP, where present is 1950) at annual resolution well into the last glacial (Figure 1).

The NH_4^+ ice concentration in Greenland represents a convolved signal of changes in emissions, transport and aerosol deposition. To go beyond previous attempts to interpret ice core aerosol records, we provide first-order reconstructions of the atmospheric aerosol concentration over the ice sheet and in the NA source region, the latter directly reflecting changes in NH_4^+ emissions (for details of the toolkit used for atmospheric aerosol reconstruction see Methods and Supplementary Information). In short, using recent NH_4^+ observations in Greenland snow and atmospheric aerosol, the effect of local deposition can be corrected for to translate snow concentration into atmospheric aerosol concentration over the ice sheet. Making first-order assumptions about past changes in lifetime/washout of NH_4^+ aerosols along its transport path, we derive an estimate of the aerosol concentration in the source region. To account for the uncertainty in our simple model, we performed sensitivity tests and rigorous error propagation. This includes the uncertainty in the deposition over the ice sheet, the transport time and atmospheric lifetime en route, providing upper and lower limits for our atmospheric reconstruction at the source (Figures 1-4).

The NGRIP NH_4^+ ice concentrations in Figure 1 show interannual variability larger than the average glacial/interglacial changes. Superimposed on this high-frequency variability are significant long-term variations. Throughout the record, pronounced positive outliers caused by biomass burning events can also be detected. The relative interannual variability is much more pronounced in extended warm periods (Figures 2-4 and S3), implying that fire and soil activity were not only higher but also more variable

in these periods. We will discuss the changes in NH_4^+ background soil emissions separately from the change in the frequency of fire peaks. To this end, we use the peak-insensitive running median in a 101-yr window to quantify changes in background concentrations at the source derived from soil emissions and use a robust outlier detection method (see Methods and Supplementary Information) to identify fire peaks in the source concentration, quantify their concentration above the corresponding background and calculate the FPF. Performing both positive and negative outlier detection relative to the running median, we can correct the positive outlier count for the small number of positive outliers, which, implied by statistics, occur in the distribution of annual concentrations but are actually derived from extraordinarily high soil emissions. Accordingly, we are confident that we essentially identify only fire events in our peak count.

Long-term changes in North American NH_4^+ soil emissions

The atmospheric aerosol reconstruction in Figure 1 demonstrates that on orbital timescales the relative changes in NH_4^+ background concentrations at the source are covariant with those in the ice. This shows that the long-term evolution of the NH_4^+ record is not controlled by transport and/or deposition effects but by source emission changes. The relative amplitudes of the observed variations are larger at the source than in the ice. The absolute amplitudes are dependent on the assumptions made for the change in atmospheric lifetime, however, the dependence of the temporal evolution in the relative changes in NH_4^+ emissions on these assumptions is small. In our best-guess reconstruction, the NGRIP NH_4^+ ice concentrations increased by a factor of 3-5 during the last glacial/interglacial transition but by a factor of ~10 in atmospheric aerosol concentrations at the source. Note that such a change is also seen in organic acid aerosol

components[23] and in NO_3^-[9], which are also of NA biogenic origin, but is opposite to that of sea salt or mineral dust aerosol[8,9]. During the glaciation into Marine Isotope Stage (MIS) 4 (70-80,000 yr ago), a NH_4^+ decline by approximately the same factor is observed.

This indicates that the NH_4^+ background concentrations from soil emissions slowly but strongly increase during long-lasting warm climate conditions. We attribute this to a general northward retreat of the ice sheet, enlarging the area of vegetation and soil formation but also bringing the NH_4^+ sources closer to Greenland. However, when reducing the atmospheric transport time in our reconstruction by 50%, transport changes still cannot explain the large glacial/interglacial variations. Accordingly, we mainly ascribe the long-term increase in soil emissions to the expansion of the NH_4^+ source area. A similar slow increase with warmer climate conditions is seen in the excess concentration from wildfires (Figures 2-4). This increase similarly reflects in part the increasing proximity of wildfires to Greenland but may also be affected by larger fire intensity due to greater fuel availability, the larger area of burnable vegetation or a change in fire type. In contrast, a direct impact of rapid temperature changes during DO events on NA soil emissions appears to be only of secondary importance, as the NH_4^+ background concentration at the source does not respond directly to the rapid DO warming. A delayed soil response in slowly thawing permafrost regions, however, cannot be excluded. Accordingly, the long-term changes in NH_4^+ and other biogenic aerosol tracers[23] can be regarded as an indirect indicator of ice sheet area variations, suggesting that the vegetated area in NA during MIS 5c and 5a was comparable to or slightly smaller than during the early Holocene. Vice versa, the vegetated area in MIS5b was slightly larger than in MIS 2-4. Taking our data at face value, soil NH_4^+ emissions, thus vegetated area, changed little during MIS2-4 (Figures 2&3).

Most of the stadial/interstadial variations seen in the source concentration are still within the uncertainty estimate of our reconstruction. However, the longest DO events (8, 12, 14 and 16) show a slow and delayed increase in average NH_4^+ source concentrations of up to a factor of about 2. In contrast, mineral dust (Ca^{2+}), sea salt (Na^+) (Figure 1) and SO_4^{2-} aerosol (Figures 2-4) show an immediate, much stronger decline during rapid warmings. The difference between NH_4^+ and SO_4^{2-} is especially noteworthy, as basic NH_3 is neutralized and transported in acidic SO_4^{2-} aerosol. This decoupling shows that it is not the availability of acidic SO_4^{2-} aerosols in the past atmosphere that controls the atmospheric NH_4^+ concentration in Greenland but rather total NH_4^+ emissions. We suggest the interstadial increase is again due to the areal shrinkage of the NA Ice Sheet (NAIS) during these very long Greenland Interstadials, as also imprinted in sea level reconstructions[3].

Stadial/interstadial changes in North American fire frequency

In contrast to the NH_4^+ background source concentrations from soil emissions, the FPF shows a clear and immediate response to most DO events during MIS3, with an approximate tripling of NH_4^+ peak frequency (Figure 2). Note that this increase may be even more pronounced for the longest DO events, where the smallest fire events cannot be detected anymore due to the concurrent increase in interannual variability in NH_4^+ source concentrations. As DO events are also times of higher annual ice layer thickness and resolution of our NH_4^+ record, we tested the validity of this result extensively (see Supplementary Information). All tests support the robustness of our results for FPF changes during MIS3.

A higher frequency of NH_4^+ peaks in parallel to DO warming may reflect an increase in the recurrence of large fire events but could also be attributed to more favourable transport conditions from NA to Greenland for these wildfire events. The general atmospheric flow pattern in MIS2-4 is largely controlled by the presence of the NAIS[26], which does not alter substantially during short DO events. Nevertheless, model experiments indicate that rapid stadial/interstadial reorganizations of atmospheric circulation over the North Atlantic occur over areas where sea ice changes[27,28]. Deuterium excess ice core observations during the Bølling-Allerød/Younger Dryas oscillation also suggest that rapid changes in sea ice led to an increased transport of more local atmospheric water vapour to Greenland[29]. However, the effect on NH_4^+ aerosol from continental sources remains unknown and other aerosol species such as mineral dust, sea salt and sulphate suggest a decline in aerosol transport to Greenland during interstadials. In view of the lack of any immediate response of the NH_4^+ background concentrations to such potential DO-related transport changes, which would affect soil and wildfire emissions similarly, the increased FPF during MIS3 interstadials is unlikely to be caused by improved transport to Greenland. Note that prior to DO20 (Figure 3), when NA glaciation was still only moderate, no clear increase in FPF can be found during DO events. However, the significantly higher interannual variability in the background NH_4^+ concentrations limits the quantitative detection of fire peaks during this period.

Independent evidence for a change in wildfire emissions and recurrence may come from the charcoal fire record. Despite the fact that the climate imprint of DO events was quite different in the northern and southern hemisphere[30], a global synthesis of charcoal concentrations suggests stronger interstadial wildfire emissions, especially for DO8 and

DO20[1], when our FPF indicates higher fire recurrence rates. Higher fire excess concentrations can also be detected in our record at those times, suggesting higher pyrogenic emissions. In contrast, higher fire activity at the end of MIS4, as suggested by the global charcoal synthesis, is not found in our NA fire frequency record. Unfortunately, no charcoal information during MIS3 exists for NA. The closest analogue is the rapid Bølling-Allerød (BA) warming, when the NAIS was still expanded[15]. The background NH_4^+ concentration at the source and the excess NH_4^+ concentration of fire peaks show a slow increase after the onset of the BA (Figure 4), which is (similar to MIS3 interstadials) delayed with respect to the rapid warming. The fire excess concentration stabilizes after about 500 yr into the BA and shows only a minor decrease during the Younger Dryas (YD), after which it slowly increases again. This temporal evolution of average NH_4^+ emissions for fire events from 15-10 kyr BP is overall in line with the NA charcoal flux record[15], despite the fact that our record is more sensitive to fires closer to Greenland. In contrast, our FPF record displays a temporal evolution quite different from that of charcoal peak density[15]. With the superior counting statistics and resolution of our FPF record compared to the NA charcoal density record, the FPF shows a rather immediate response to the BA climate variations and a clear YD minimum, similar to the FPF response during MIS3 stadials. The FPF change at the onset of the BA warming would be even more pronounced if small fire events were still detectable, however the increase in interannual variability prevents their identification. Again, the observed FPF change indicates a strong direct response of fire recurrence to rapid warmings, which appears to be most pronounced at the onset of the BA and at the end of the YD (Figure 4), potentially fuelled by an increased mortality of pre-existing vegetation in response to rapid climate change.

Our NGRIP record allows us to reconstruct both NH_4^+ background concentrations from NA soil emissions and wildfire frequency over the entire last glacial cycle, however, an aerosol tracer reflecting only biomass burning is desirable to also add specific information on fire emission strengths. While levoglucosan[16] shows high potential, it is not available at the same resolution as NH_4^+ records, crucial for quantifying fire recurrence rates. Our record shows that soil NH_4^+ emissions are higher for warm interglacial conditions due to the expansion of vegetation, while during glacial times NH_4^+ emissions are suppressed by the larger NA ice cover. The response of NH_4^+ soil emissions to rapid DO warmings is very limited and delayed, indicating that rapid temperature changes during DO events are not the controlling factor for NA nitrogen soil turnover, however the frequency for fire occurrence increases during rapid warmings.

Methods

NH_4^+ concentrations were measured on the NGRIP ice core on ice rods with a square cross section of about 10 cm^2 using our Continuous Flow Analysis (CFA) system[18,24] and complemented by previously published CFA data from the GRIP ice core[18]. Note that NH_4^+ measurements on discrete samples using classical ion chromatographic analysis are prone to NH_3 contamination by lab air and only CFA analysis provides the environment for reliable NH_4^+ measurements for the very low concentrations found in Greenland ice. Quantification of the NH_4^+ ice concentrations is based on a fluorimetric method using the reaction of NH_4^+ with o-phthaldialdehyde. The limit of detection of this method is 0.1 ng/g, the uncertainty of the measured concentration is always smaller than 0.4 ng/g[20,24]. The data are sampled in 1 mm resolution, however due to dispersion in the CFA system the true achievable resolution is 1.2 cm[25]. The NGRIP NH_4^+ raw data

were down-sampled to nominal annual averages according to the extended GICC05 age scale[31-33], the latter being based on multi-parameter layer counting down to 60 kyr BP and extended by a glaciological flow model for older ages. The nominal annual averages in NH_4^+ do not reflect annual means from one seasonal NH_4^+ minimum to the next but are defined by the available age scale. Moreover, layer counting based on NH_4^+ concentrations cannot be achieved throughout the record due to the maximum resolution of the CFA measurement and because the annual layer thickness is reduced for colder periods due to lower precipitation and generally declines with increasing depth due to glacier flow. This translates into a decreasing temporal resolution of the record with depth (Figure S4). Seasonal variations in the NGRIP NH_4^+ record can be clearly resolved for the late glacial/interglacial transition. The maximum resolution during DO events in MIS3 and the Last Glacial Maximum is 0.3-0.5 years and about one year for stadials in MIS3. In older ice only the warmest periods may allow for a maximum resolution of 1 year, while stadial resolutions are lower than 1 year (see also Supplementary Information).

To calculate the atmospheric aerosol concentration in Greenland from concentrations in the ice, we corrected for the effect of dry and accumulation-dependent wet deposition, using dry deposition velocities and scavenging ratios from literature values[34,35] and using an extended data set of spatial variations in mean NH_4^+ concentrations in shallow Greenland ice cores. Using the derived atmospheric concentration over the ice sheet we back-calculated the atmospheric aerosol concentration over the NA source region assuming an exponential decline from the source to the ice sheet dependent on transport time and atmospheric lifetime. To determine the recent NH_4^+ transport time to Greenland we calculated a back-trajectory climatology for the NEEM ice core site[36]

(assuming comparable transport conditions for NEEM and NGRIP) using only trajectories originating in the NA continental boundary layer and ending at NEEM. For the recent atmospheric lifetime of NH_4^+ en route we used the value by Dentener&Crutzen[19]. For the past we scaled the recent wet deposition (which is dependent on the total precipitation en route derived from the back-trajectory climatology) by the relative temporal change in accumulation rate at NGRIP. In order to account for the considerable uncertainties in this simple approach, we performed rigorous error propagation, including the uncertainty in the atmospheric lifetime en route as well as in the dry deposition velocity and the scavenging ratio over the ice sheet. Moreover, we tested the sensitivity of the results to changes in transport time (for details see Supplementary Information).

Finally, we separated background NH_4^+ concentrations derived from NA soil emissions from positive NH_4^+ outliers caused by NA biomass burning events. To quantify the background concentrations we used the running median in a 101 yr window as this robust measure is insensitive to a few years affected by wildfires. To identify the biomass burning events we used a threshold above the running median defined by three times the median of the absolute deviation from the median (MAD) in the 101 yr window. Using these identified peaks we were able to calculate peak frequencies. Assuming a symmetric lognormal distribution of the annual background concentrations around the median we were able to correct our peak count for the very small number of randomly occurring large peaks from soil emissions. This corrected peak count is always smaller than 20 per 201 year window and thus very similar (or in cold intervals even smaller) than the number of fire peaks unambiguously identified using other chemical

fire tracers[17]. Accordingly, with this approach we are confident that our corrected peak count is a reliable measure of fire peak frequency only.

The new annual resolution NH_4^+ concentrations and the data on spatial variations in average NH_4^+ ice concentrations in Greenland over the last centuries are available as supplementary tables of this publication.

GISP2 ion data[9] are available at:

ftp://ftp.ncdc.noaa.gov/pub/data/paleo/icecore/greenland/summit/gisp2/chem/iond.txt

GRIP NH4+ data are available at:

ftp://ftp.ncdc.noaa.gov/pub/data/paleo/icecore/greenland/summit/grip/chem/nh4.txt

NGRIP $\delta^{18}O$ data[4] and age scales for Greenland ice cores synchronized to the extended GICC05 age scale[37] are available at: http://www.iceandclimate.nbi.ku.dk/data

NGRIP ice core accumulation rates[5] are available at:

http://www.clim-past.net/10/887/2014/cp-10-887-2014-supplement.zip

The Red Sea sea level reconstruction[3] is available at:

http://www.nature.com/nature/journal/v491/n7426/full/nature11593.html

Charcoal compilation for North America over the last glacial/interglacial transition[15] is part of the Global Charcoal Data Base: https://www.ncdc.noaa.gov/paleo/impd/gcd.html. The compilation can be downloaded directly at : http://jennmarlon.info/papers/Marlon_etal_2012_PNAS_figure%20data.zip

References

1 Daniau, A.-L., Harrison, S. P. & Bartlein, P. J. Fire regimes during the Last Glacial. *Quat Sci Rev* **29**, 2918–2930, doi:10.1016/j.quascirev.2009.11.008 (2010).

2 McConnell, J. R. *et al.* 20th-Century Industrial Black Carbon Emissions Altered Arctic Climate Forcing. *Science* **317**, 1381-1384, doi:10.1126/science.1144856 (2007).

3 Grant, K. M. *et al.* Rapid coupling between ice volume and polar temperature over the past 150,000 years. *Nature* **491**, 744-747, doi:10.1038/nature11593 (2012).

4 North Greenland Ice Core Project members. High resolution climate record of the northern hemisphere reaching into the last interglacial period. *Nature* **431**, 147-151, doi:10.1038/nature02805 (2004).

5 Kindler, P. *et al.* Temperature reconstruction from 10 to 120 kyr b2k from the NGRIP ice core. *Climate of the Past* **10**, 887–902, doi:10.5194/cp-10-887-2014 (2014).

6 Baumgartner, M. *et al.* NGRIP CH4 concentration from 120 to 10 kyr before present and its relation to a $\delta^{15}N$ temperature reconstruction from the same ice core. *Clim. Past* **10**, 903-920, doi:10.5194/cp-10-903-2014 (2014).

7 Wang, Y. *et al.* Millennial- and orbital-scale changes in the East Asian monsoon over the past 224,000 years. *Nature* **451**, 1090-1093, doi:10.1038/nature06692 (2008).

8 Fischer, H., Siggaard-Andersen, M.-L., Ruth, U., Röthlisberger, R. & Wolff, E. Glacial/Interglacial changes in mineral dust and sea salt records in polar ice cores: sources, transport, deposition. *Rev Geophys* **45**, RG1002, doi:1010.1029/2005RG000192 (2007).

9 Mayewski, P. A. *et al.* Major features and forcing of high-latitude northern hemisphere atmospheric circulation using a 110,000-year-long glaciochemical series. *J Geophys Res* **102**, 26345-26366 (1997).

10 Jimenez-Moreno, G. *et al.* Millennial-scale variability during the last glacial in vegetation records from North America. *Quat Sci Rev* **29**, 2865–2881, doi:10.1016/j.quascirev.2009.12.013 (2010).

11 Asmerom, Y., Polyak, V. J. & Burns, S. J. Variable winter moisture in the southwestern United States linked to rapid glacial climate shifts. *Nature Geoscience* **3**, 114 - 117, doi:10.1038/NGEO754 (2010).

12 Sionneau, T. *et al.* Atmospheric re-organization during Marine Isotope Stage 3 over the North American continent: sedimentological and mineralogical evidence from the Gulf of Mexico. *Quat Sci Rev* **81**, 62-73, doi:10.1016/j.quascirev.2013.10.002 (2013).

13 Whitlock, C. & Bartlein, P. J. Vegetation and climate change in northwest America during the past 125 kyr. *Nature* **388**, 57-61 (1997).

14 Grimm, E. C., Jacobson, G. L., Watts, W. A., Hansen, B. C. S. & Maasch, K. A. A 50,000-year record of climate oscillations from Florida and its temporal correlation with the Heinrich events. *Science* **261**, 198-200 (1993).

15 Marlon, J. R. *et al.* Wildfire responses to abrupt climate change in North America. *Proceedings of the National Academy of Sciences* **106**, 2519–2524, doi:10.1073/pnas.0808212106 (2009).

16 Zennaro, P. *et al.* Fire in ice: two millennia of boreal forest fire history from the Greenland NEEM ice core. *Climate of the Past* **10**, 1905–1924, doi:10.5194/cp-10-1905-2014 (2014).

17 Savarino, J. & Legrand, M. High northern latitude forest fires and vegetation emissions over the last millennium inferred from the chemistry of a central Greenlabd ice core. *J Geophys Res* **103**, 8267-8279 (1998).
18 Fuhrer, K., Neftel, A., Anklin, M., Staffelbach, T., Legrand, M. High resolution ammonium ice core record covering a complete glacial-interglacial cycle. *J Geophys Res* **101**, 4147-4164 (1996).
19 Dentener, F. J. & Crutzen, P. J. A Three-Dimensional Model of the Global Ammonia Cycle. *Journal of Atmospheric Chemistry* **19**, 331-369 (1994).
20 Gfeller, G. *et al.* Representativeness of major ions measurements and seasonality derived from NEEM firn cores. *The Cryosphere* **8**, 1855–1870, doi:10.5194/tc-8-1855-2014 (2014).
21 Kehrwald, N. *et al.* Levoglucosan as a specific marker of fire events in Greenland snow. *Tellus B* **64**, 18196, 18110.13402/tellusb.v18164i18190.18196 (2012).
22 Jaffrezo, J.-L. *et al.* Biomass burning signatures in the atmosphere of central Greenland. *J Geophys Res* **103**, 31067-31078 (1998).
23 Legrand, M. & De Angelis, M. Light carbolyxic acids in Greenland ice: A record of past forest fires and vegetation emissions from the boreal zone. *J Geophys Res* **101**, 4129-4145 (1996).
24 Röthlisberger, R. *et al.* Technique for continuous high-resolution analysis of trace substances in firn and ice cores. *Environmental Science and Technology* **34**, 338-342, doi:10.1021/es9907055 (2000).
25 Kaufmann, P. *et al.* An improved Continuous Flow Analysis (CFA) system for high-resolution field measurements on ice cores. *Environmental Science & Technology* **42**, 8044-8050, doi:10.1021/es8007722 (2008).
26 Pausata, F. S. R., Li, C., Wettstein, J. J., Kageyama, M. & Nisancioglu, K. H. The key role of topography in altering North Atlantic atmospheric circulation during the last glacial period. *Climate of the Past* **7**, 1089–1101, doi:10.5194/cp-7-1089-2011 (2011).
27 Kageyama, M. *et al.* Glacial climate sensitivity to different states of the Atlantic Meridional Overturning Circulation: results from the IPSL model. *Climate of the Past* **5**, 551–570 (2009).
28 Zhang, X., Lohmann, G., Knorr, G. & Purcell, C. Abrupt glacial climate shifts controlled by ice sheet changes. *Nature* **512**, 290-294, doi:10.1038/nature13592 (2014).
29 Steffensen, J. P. *et al.* High-resolution Greenland ice core data show abrupt climate change happens in few years. *Science* **321**, 680-684, doi:10.1126/science.1157707 (2008).
30 EPICA community members. One-to-one coupling of glacial climate variability in Greenland and Antarctica. *Nature* **444**, 195-198 (2006).
31 Wolff, E. W., Chappellaz, J., Blunier, T., Rasmussen, S. O. & Svensson, A. Millennial-scale variability during the last glacial: The ice core record. *Quat Sci Rev* **29**, 2828–2838, doi:10.1016/j.quascirev.2009.10.013 (2010).
32 Rasmussen, S. O. *et al.* A new Greenland ice core chronology for the last glacial termination. *J Geophys Res* **111**, D06102, doi:06110.01029/02005JD006079 (2006).
33 Svensson, A. *et al.* A 60 000 year Greenland stratigraphic ice core chronology. *Climate of the Past* **4**, 47-57 (2008).
34 Bergin, M. H. *et al.* The contributions of snow, fog, and dry deposition to the summer flux of anions and cations at Summit, Greenland. *J Geophys Res* **100**, 16275-16288 (1995).

35 Davidson, C. I., Bergin, M. H. & Kuhns, H. D. in *Chemical exchange between the atmosphere and polar snow* Vol. 43 *NATO ASI Series* (eds E.W. Wolff & Bales R.C.) 275-306 (Springer Verlag, 1996).
36 NEEM community members. Eemian interglacial reconstructed from a Greenland folded ice core. *Nature* **493**, 489-494, doi:10.1038/nature11789 (2013).
37 Seierstad, I. K. *et al.* Consistently dated records from the Greenland GRIP, GISP2 and NGRIP ice cores for the past 104 ka reveal regional millennial-scale $\delta^{18}O$ gradients with possible Heinrich event imprint. *Quat Sci Rev* **106**, 29-46, doi:10.1016/j.quascirev.2014.10.032 (2014).
38 Rasmussen, S. O. *et al.* A stratigraphic framework for abrupt climatic changes during the Last Glacial period based on three synchronized Greenland ice-core records: refining and extending the INTIMATE event stratigraphy. *Quat Sci Rev* **106**, 14-28, doi:10.1016/j.quascirev.2014.09.007 (2014).

Correspondence and requests for materials should be addressed to HF (hubertus.fischer@climate.unibe.ch).

Acknowledgments

The authors of this paper are indebted to the late Dietmar Wagenbach, who contributed to and inspired this research in numerous discussions. This paper has also greatly benefitted from the Sir Nicholas Shackleton fellowship, Clare Hall, University of Cambridge, U.K., awarded to HF in 2014. The Division for Climate and Environmental Physics, Physics Institute, University of Bern acknowledges the long-term financial support of ice core research by the Swiss National Science Foundation (SNSF) and the Oeschger Centre for Climate Change Research. EW is supported by a Royal Society professorship. NGRIP is directed and organized by the Department of Geophysics at the Niels Bohr Institute for Astronomy, Physics and Geophysics, University of Copenhagen. It is supported by funding agencies in Denmark (SNF), Belgium (FNRS-CFB), France (IPEV and INSU/CNRS), Germany (AWI), Iceland (RannIs), Japan (MEXT), Sweden (SPRS), Switzerland (SNSF) and the USA (NSF, Office of Polar Programs).

Author contributions

M.B. and R.R. performed the CFA measurements in the field at NGRIP and together with S.S. carried out raw data analysis. H.F. developed the time series analysis approach and together with R.M. and E.W. the concept for reconstruction of atmospheric concentrations. G.G. provided back trajectory analysis used in the transport model, T.E. contributed to the deposition model. All authors discussed the results and contributed to the interpretation and to the manuscript, which was written by H.F.

Competing financial interests

The authors declare no competing financial interests.

Figure Captions:

Figure 1: Climate and environmental changes recorded in Greenland ice cores – a sea salt (Na^+) and mineral dust (Ca^{2+}) aerosol concentrations in the GISP2 ice core; **b** stable water isotope temperature proxy in the NGRIP ice core[4] ($\delta^{18}O$ expressed in ‰ with respect to Vienna Standard Mean Ocean Water); **c** annual NH_4^+ concentration in the NGRIP ice core (grey) together with the 101 yr running median (orange) representing background concentrations; **d** atmospheric background NH_4^+ aerosol concentrations over the ice sheet (orange), together with its uncertainty band (light blue); **e** atmospheric background NH_4^+ aerosol concentration at the NA source from soil emissions (orange), together with its uncertainty band (light blue); **f** the atmospheric aerosol lifetime in days (black) controlled by the change in precipitation rate[5]; **g** relative sea level reconstruction based on Red Sea sediments (dark blue) together with its 95% confidence band (grey)[3]. All ice core derived data are displayed on the model extended GICC05 age scale[37], the sea level reconstruction is given on its own age scale.

Figure 2: High-resolution records of NH_4^+ soil emissions and wildfire activity in NA during MIS3 – a fire event concentrations (red dots) at the source in excess of the background concentrations. The grey line indicates the detection threshold for fire events; **b** atmospheric background NH_4^+ aerosol concentration from soil emissions at the NA source (101 yr running median, orange) together with its uncertainty band (light blue); **c** NH_4^+ background ice concentration in the NGRIP (101 yr running median, light orange) and the GRIP ice cores[18] (55 cm averages, grey); **d** DO variability in the NGRIP stable water isotope proxy during MIS3[5]; **e** SO_4^{2-} concentration in the GISP2 ice core[9]; **f** corrected fire peak frequency (FPF, purple) per 201 yr window. Warm Greenland Interstadials (GI) are indicated by numbers[38], cold stadials by light blue bars.

Figure 3: High-resolution records of NH_4^+ soil emissions and wildfire activity in NA during MIS4 and MIS5b - a-f same as in Figure 2.

Figure 4: High-resolution records of NH_4^+ soil emissions and wildfire activity in North America during the last glacial/interglacial transition - a-f same as in Figure 2; **g** NA charcoal influx compilation (brown) and **h** NA charcoal peak density (green) by Marlon et al.[15] on their own age scale.

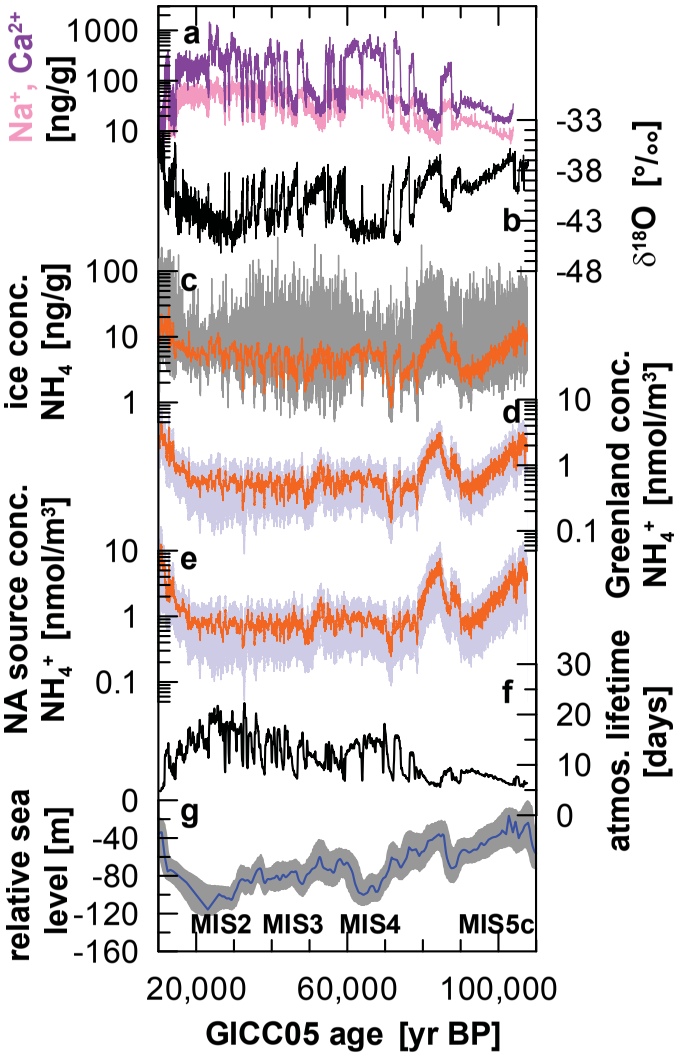
Na+, Ca2+ [ng/g]
1000
100
10
a
b
-33
-38
-43
-48
δ18O [°/oo]
ice conc. NH4 [ng/g]
100
10
1
c
d
10
1
0.1
Greenland conc. NH4+ [nmol/m3]
NA source conc. NH4+ [nmol/m3]
10
1
0.1
e
f
30
20
10
0
atmos. lifetime [days]
relative sea level [m]
0
-40
-80
-120
-160
g
MIS2
MIS3
MIS4
MIS5c
20,000
60,000
100,000
GICC05 age [yr BP]

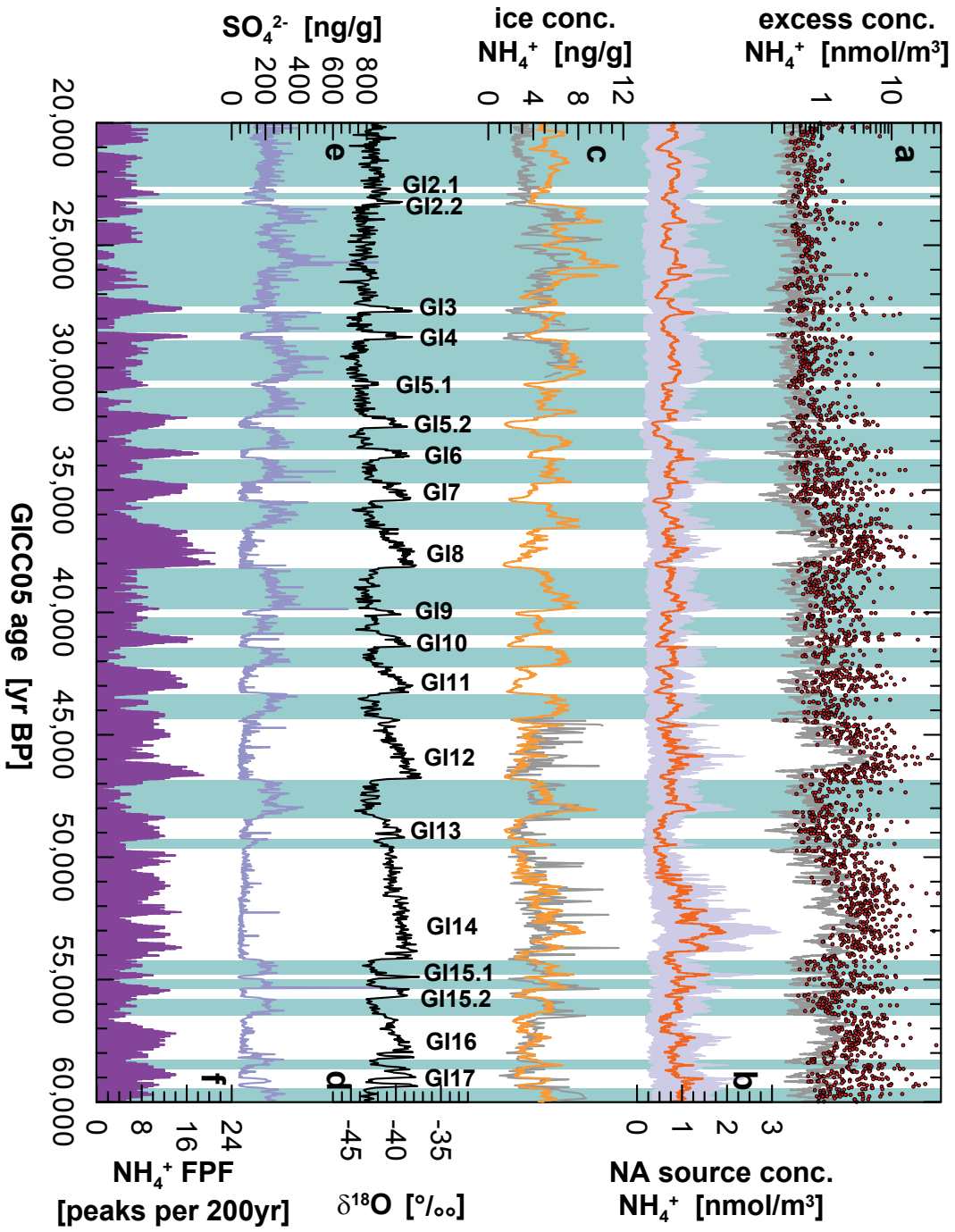
excess conc.
NH4+ [nmol/m3]
ice conc.
NH4+ [ng/g]
SO4 2- [ng/g]
GICC05 age [yr BP]
GI2.1
GI2.2
GI3
GI4
GI5.1
GI5.2
GI6
GI7
GI8
GI9
GI10
GI11
GI12
GI13
GI14
GI15.1
GI15.2
GI16
GI17
NA source conc.
NH4+ [nmol/m3]
δ18O [°/oo]
NH4+ FPF
[peaks per 200yr]

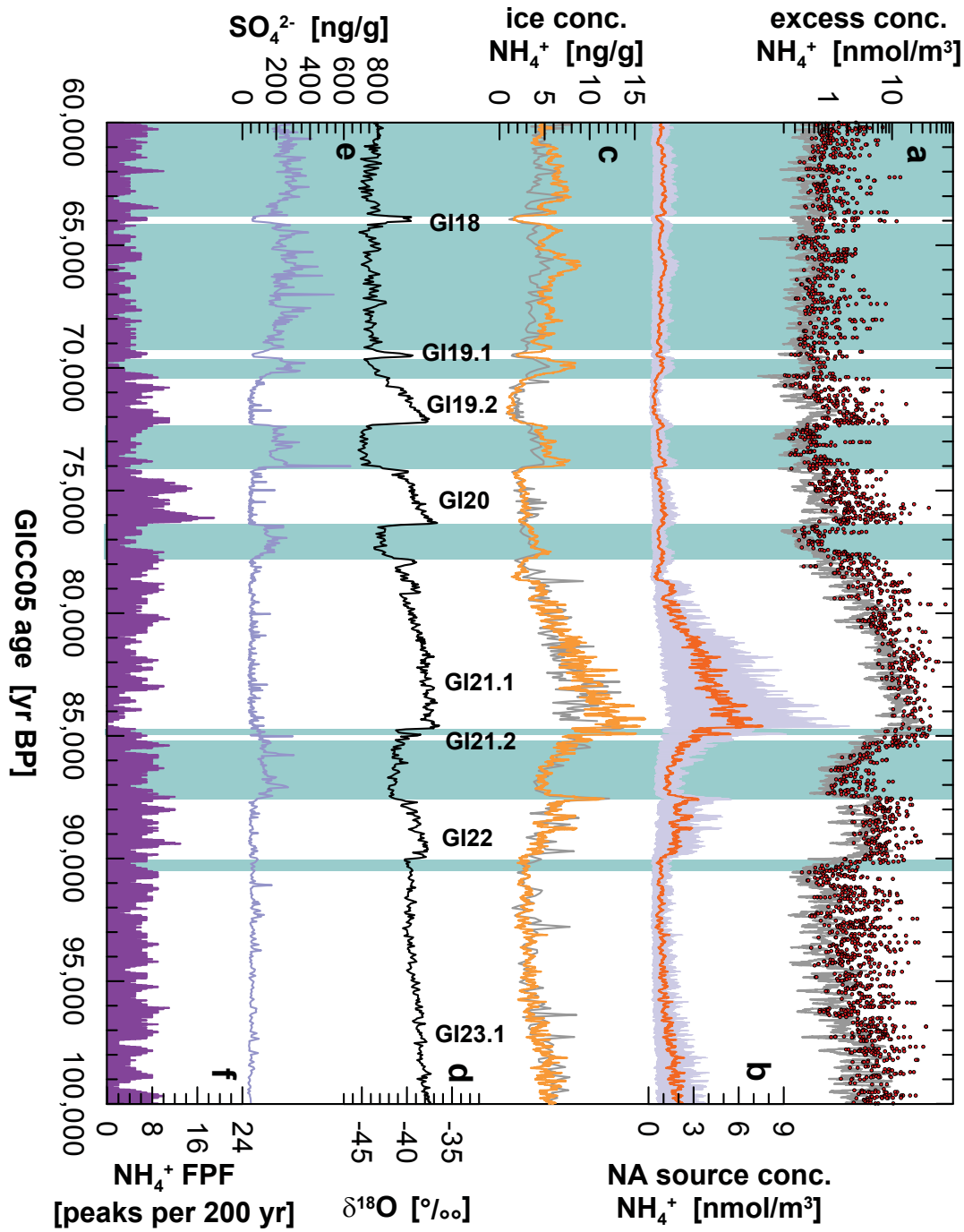
excess conc.
NH4+ [nmol/m3]
ice conc.
NH4+ [ng/g]
SO4 2- [ng/g]
a
b
c
d
e
f
GI18
GI19.1
GI19.2
GI20
GI21.1
GI21.2
GI22
GI23.1
GICC05 age [yr BP]
NA source conc.
NH4+ [nmol/m3]
δ18O [°/oo]
NH4+ FPF
[peaks per 200 yr]

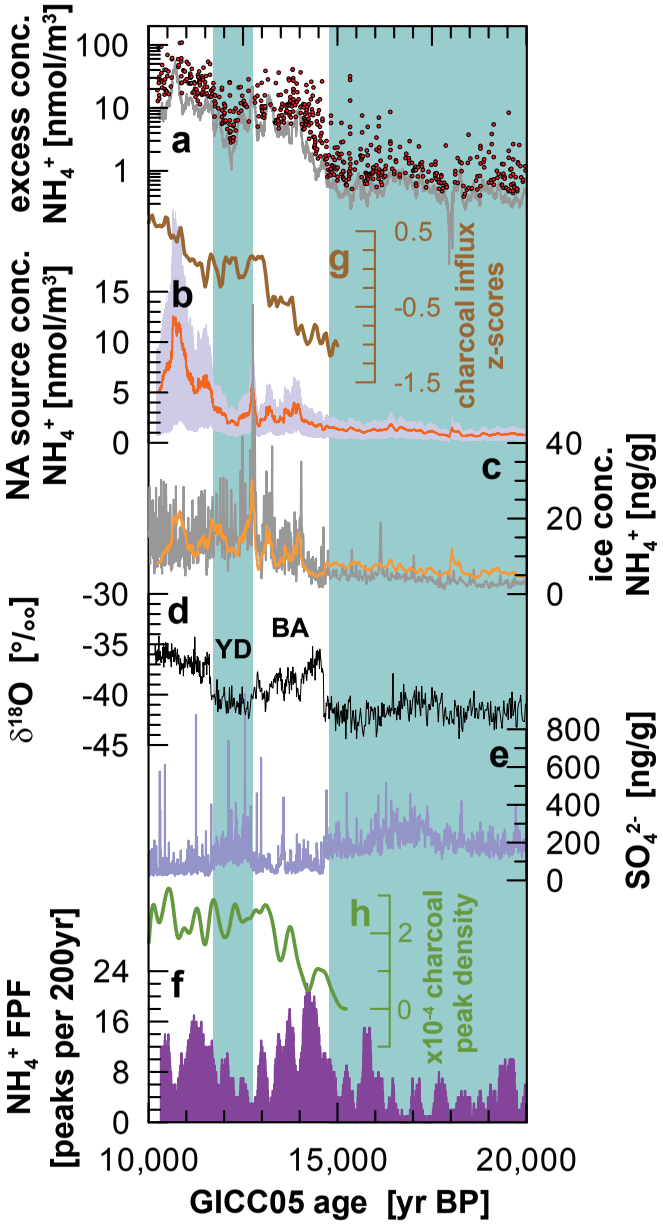
excess conc. NH4+ [nmol/m3]
100
10
1
a
NA source conc. NH4+ [nmol/m3]
15
10
5
0
b
g
0.5
-0.5
-1.5
charcoal influx z-scores
c
40
20
0
ice conc. NH4+ [ng/g]
δ18O [°/oo]
-30
-35
-40
-45
d
YD
BA
e
800
600
400
200
0
SO4 2- [ng/g]
NH4+ FPF [peaks per 200yr]
24
16
8
0
f
h
2
0
x10-4 charcoal peak density
10,000
15,000
20,000
GICC05 age [yr BP]

Supplementary Information to

Millennial changes in North American wildfire and soil activity over the last glacial cycle

Hubertus Fischer[1], Simon Schüpbach[1], Gideon Gfeller[1], Matthias Bigler[1], Regine Röthlisberger[1], Tobias Erhardt[1], Thomas F. Stocker[1], Robert Mulvaney[2], Eric W.Wolff[3]

[1] Climate and Environmental Physics, Physics Institute & Oeschger Centre for Climate Change Research, University of Bern, Sidlerstrasse 5, 3012 Bern, Switzerland, hubertus.fischer@climate.unibe.ch

[2] British Antarctic Survey, Cambridge, U.K.

[3] Department of Earth Sciences, Cambridge University, Cambridge, U.K.

Toolkit for the reconstruction of atmospheric concentrations

The NH_4^+ concentrations in an ice core represent a convoluted signal of changes in emission, changes in transport and deposition en route as well as local deposition changes over the ice sheet due to varying contributions of wet and dry deposition. In order to translate ice concentrations to local atmospheric aerosol concentrations over the ice sheet, both the effective dry deposition velocity and the scavenging ratio for wet deposition need to be known. Very limited direct observations exist for the top of the Greenland ice sheet. Direct measurements of the dry deposition velocity in Central Greenland at Summit for summer gave values of 0.017±0.011 cm/s[1] and similar values for Dye 3 on the Southern Greenland ice sheet[2]. The mass scavenging ratio has been determined for SO_4^{2-} aerosol for summer conditions as 220±130[2], again with similar values for Dye 3. No scavenging ratios are explicitly quantified for NH_4^+ in that study, but as NH_4^+ is incorporated in acidic SO_4^{2-} aerosol, it is safe to assume a similar value for NH_4^+. The measured NH_4^+ aerosol concentration at Summit during summer[1], where soil and biomass burning emissions are the strongest, is highly variable (reflecting events of NH_4^+ transport to Greenland) within a range of 0.5-10 nmol/m^3[3]. Averaged over the entire year the NH_4^+ aerosol concentration is expected to be at the lower bound of this range and we estimate an average annual NH_4^+ aerosol concentration on the ice sheet in the order of 1.5±1.0 nmol/m^3.

Given the high variability and the limited temporal and seasonal coverage of the direct atmospheric observations described above, we tried to get more robust values of the dry deposition velocity and scavenging ratio making use of our extended CFA ice core data set of NH_4^+ concentrations in Greenland snow and ice over a very wide range of accumulation rates covering several centuries back in time. As there are no significant

temporal trends found in NH_4^+ concentrations in Greenland ice cores over the last few centuries, we can directly compare averages from ice cores from climatologically different regions on the ice sheet to derive temporally more robust deposition parameters. Moreover, given the lack of a clear anthropogenic signal, the rather distant source of NH_4^+ in continental NA implies rather homogenous atmospheric NH_4^+ aerosol concentrations on the Greenland plateau, where our firn and ice cores were drilled. Averaged over a sufficient time period, the snow concentration C_{ice} in Greenland firn is connected to the atmospheric aerosol concentration C_{air} via the dry deposition velocity v_{dry} and the mass scavenging ratio ε according to[1,3]

$$C_{ice}(\mathrm{NH_4^+}) = \varepsilon C_{air}(\mathrm{NH_4^+}) + \frac{v_{dry} C_{air}(\mathrm{NH_4^+})}{A} \qquad (1)$$

where A is the average accumulation rate, which is representative of the mean precipitation rate at the ice core drill site. A two-sided linear regression of the average NH_4^+ concentration of each individual core C_{ice} with the inverse mean accumulation rate (Figure S1) at each site for our extended data set of Greenland firn cores, leads to

$$C_{ice}(\mathrm{NH_4^+}) = (3.9 \pm 0.7)\left[\frac{\mathrm{ng}}{\mathrm{g}}\right] + (47.75 \pm 9.51)\frac{1}{A}\left[\frac{\mathrm{ng}}{\mathrm{g}}\frac{\mathrm{cmWE}}{\mathrm{yr}}\right]; \quad r^2 = 0.53$$

Using the mean annual atmospheric NH_4^+ aerosol concentration over the ice sheet and its uncertainty given above, this leads to a long-term annual average in dry deposition velocity of v_{dry}=0.056±0.039 cm/s and in mass scavenging ratio of ε=138±95, which are in the same range as the short-term direct atmospheric summer observations above. In the following we assumed these ice core derived values to be constant back in time and used them to calculate past atmospheric NH_4^+ concentrations over the ice sheet. To account for the considerable uncertainty in these parameters, we used Gaussian error propagation to get uncertainty estimates for the atmospheric NH_4^+ concentrations over the ice, where we also included the uncertainty in the reconstructed past accumulation

rate[4] estimated to be ±2 cm water equivalent (WE)/yr, i.e. 20-50% of the accumulation in MIS3. This uncertainty is given in the light blue band in Figures 1. As can be seen in Figure 2, the NH_4^+ ice concentrations are characterized by a characteristic minimum at the onset of each DO event. Our reconstruction of atmospheric concentrations over the ice sheet shows that these dips are a depositional artefact caused by the increase in precipitation at the ice core location at a time when NH_4^+ emissions were still low.

Dry and wet deposition occur also along the transport pathway from the NA NH_4^+ source regions to Greenland leading to a depletion of the atmospheric NH_4^+ load with transport time *t*, which can be estimated in a simple first order process according to

$$C_{air}(\mathrm{NH}_4^+, t) = C_{air}(\mathrm{NH}_4^+, t=0) \cdot e^{-\frac{t}{\tau}} \qquad (2)$$

where the atmospheric lifetime

$$\tau = \frac{H}{v_{dry} + \varepsilon P}$$

is controlled by the dry deposition velocity and scavenging ratio en route[5] with *H* being the thickness of the air column subject to washout and rainout of NH_4^+ bearing aerosol transported to Greenland from the NA continent. The dry deposition flux will be essentially the same along the route as the value determined over the ice sheet, since it is only dependent on the size of aerosol. However, the wet deposition during transport will be much larger, as the precipitation *P* en route is much higher than over the ice sheet. To quantify *P* for recent conditions we used a comprehensive back-trajectory analysis based on ERA-interim reanalysis data over the last 30 years for the NEEM ice core, that we recently derived and assuming similar transport and precipitation conditions en route for NEEM and NGRIP. We determined the mean annual precipitation (*P*=88±11 cm WE/yr) averaged over all trajectories that may transport NH_4^+ to NEEM,

i.e. trajectories originating in the boundary layer over the NA continent within 5-6 days prior to arrival. Using the scavenging ratio found over the ice sheet and assuming a column height of H=4000 m this would translate to a life time of NH_4^+ bearing aerosol of about 10.2 days, which is much longer than the recent lifetime of NH_4^+ of about 4.5 days[6]. This is likely due to the fact that the scavenging ratio on the ice sheet is not representative for the wet deposition along the entire transport path. Accordingly, to take this into account we increased the scavenging ratio during transport to effectively decrease the atmospheric lifetime to 4.4 days typical for recent conditions. This empiric adjustment of the lifetime also implies that the choice of the column height H becomes irrelevant. Note that the absolute amplitude of past changes in NH_4^+ concentration at the source is strongly dependent on this choice of the lifetime for recent conditions, however, the temporal evolution of the relative changes from one time period to the next is not affected as long as the scavenging ratio does not change significantly over time.

During glacial times the precipitation en route will be substantially smaller than today as also seen by up to a factor of 5 lower precipitation rates found in Greenland during that time[4]. To come up with a first order estimate, we scaled the changes in the precipitation en route from its current level to the change in the accumulation rate in Greenland in the past relative to its present value[7] (17.4 cm WE/yr) and solved equation (2) above for $C_{air}(NH_4^+,t=0)$ to derive a first order estimate of the atmospheric NH_4^+ aerosol concentration at the source. Obviously, this is only a first order estimate, but is sufficient to decipher, which variations in the measured ice concentrations are only due to depositional effects and which are due to source changes.

The relative changes in glacial/interglacial and stadial/interstadial NH_4^+ concentration at the source are strongly dependent on the choice of the scavenging ratio in this simple approach. For instance, when using the low scavenging ratios as determined over the ice sheet for the entire washout during transport (and a column height of H=4000m), the atmospheric concentrations at the source are only 60% higher than over the ice sheet, which is unrealistically low. Using the adjusted lifetime for recent conditions, the atmospheric concentrations at the source are 3 times higher than over Greenland. Interestingly, this is in line with current background NH_4^+ aerosol concentrations at Niwot Ridge[8] of about 5 nmol/m^3, providing further independent support of our choice of atmospheric lifetime for recent conditions.

In order to account for the considerable uncertainties in this simple approach, we performed rigorous error propagation for our reconstructed atmospheric concentration at the source, including the uncertainty in the dry deposition velocity, in the scavenging ratio as well as in the scaling factor to adjust atmospheric lifetime, the precipitation rate en route and in the uncertainty in the atmospheric aerosol concentration over the ice. The resulting uncertainty range is displayed as the light blue band in Figures 1-4. As the atmospheric transport path was longer during glacial times due to the larger distance of the NH_4^+ source to Greenland caused by the expanded ice cover, a longer transport time t is to be expected, although higher glacial wind speeds may have counterbalanced this effect to some extent[5,9]. Instead of including these potential, systematic changes in transport time in our error propagation, we varied t in different reconstruction runs to constrain how much of the observed variations may be explained by such a change in transport time. The result of this exercise is displayed in Figure S2. This shows that the range of source concentrations observed during MIS3 could be in principle explained by

a doubling of the transport time. However, the lack of a direct imprint of the rapid DO transitions in the source concentrations renders it very unlikely that the observed changes are due to a change in transport time, as the latter is expected to vary in parallel to DO warmings. Moreover, the glacial/interglacial changes in the source concentration at the source are much larger than could be explained by any reasonable change in transport time. Accordingly, the very high NH_4^+ source concentrations during the Holocene, MIS5a and MIS5c are not controlled by changes in transport time and must be connected to an increase in emissions due to higher nitrogen soil turnover.

Time Series Analysis

In order to describe the temporal evolution of NH_4^+ concentrations, to separate background concentrations from peaks and to derive biomass burning event frequencies, time series analysis was performed and tested for resolution effects. To describe the long-term trend in the background concentration, the running median of the logarithmic annual NH_4^+ concentration was calculated in a 101 year window (together with running percentiles on the 10%, 25%, 75% and 90% level). Occasionally missing annual values were ignored in this analysis. With increasing variability in the background concentrations the chance increases that smaller fire events are included in the background distribution. However, their number is always much smaller than the number of years solely affected by soil emissions and, therefore, this small number will not affect the running median as our robust measure of typical background concentrations. This running median is therefore representative for soil emissions and is not affected by small fire peaks. The 25% and 75% percentiles (as well as the 10% and 90% percentiles) are not symmetric around the median, indicating the increasing influence of fire peaks on the upper tail in the distribution of logarithmic annual

concentrations.

In order to separate the biomass burning peaks from the background distribution in the atmospheric concentrations at the source (see below), we calculated the running median and the median of the absolute deviation from the median[10] (MAD, an outlier insensitive measure of the variability in the data) of the logarithmic annual NH_4^+ concentrations at the source in a 101 yr window (Figure S3), thus, taking the approximately log-normal distribution of annual NH_4^+ background concentrations into account. This running approach ensures, that distribution parameters changing with time can be taken into account. As clearly seen in Figure S3, the variability in the data is substantially larger for temporally extended warm periods such as GI8, 12, 14, 16, 21 or 22, where, accordingly, less biomass burning events can be detected.

Biomass burning peaks in an individual year *i* were identified as "positive" outliers from the background distribution[11] if their annual logarithmic concentration $\log(NH_4^+(i))$ at the source exceeded a threshold given by:

$$\log(\mathrm{NH}_4^+(i)) \geq Median(i) + n \cdot MAD(i)$$

We also counted outliers on the low concentration part of the distribution of the logarithmic concentrations (further on called „negative outliers") according to

$$\log(\mathrm{NH}_4^+(i)) \leq Median(i) - n \cdot MAD(i)$$

If the background concentrations derive from an approximate lognormal distribution of annual concentration values, this negative outlier count should be small. Moreover, it can be used to correct the positive outlier count for the number of peaks that are by chance identified as positive outliers with our method but are actually derived from the lognormal background distribution itself (see below).

The factor *n* is a free parameter but should be chosen large enough in order to avoid that annual concentrations, which are part of the background distribution, are counted as outliers. A simple test for this is to look at the negative outliers, where only a few outliers should be detected. Here, we used both n=2 and n=3, which of course affected the total number of positive and negative outliers, but had a negligible effect on the relative changes in the FPF (see below). In Figures 2-4 we displayed the result for *n*=3. In this case 6878 positive outliers out of 97349 annual values have been identified, the negative outlier count was only 767, i.e., only 11% of the positive counts. It is important to note that counting the outliers directly on the ice concentrations instead of the reconstructed atmospheric concentrations at the source leads with 6825/770 positive/negative outliers to practically the same results. This is to be expected as most of our transformations only scale the absolute level of the annuals concentration but not their order, implying that these transformations are not affecting our robust median/MAD method. For *n*=2 the positive peak count was 13158, however, in this case also 4404 negative outliers (equivalent to 33% of the positive counts) were identified. This shows that with decreasing *n* more and more annual values that are not outliers but years with concentrations on the upper tail of the log-normal distribution of annual background concentrations are counted.

Nominal annual concentration values were calculated using the GICC05 age scale. This age scale is counted down to 42 kyr BP based on a multi-parameter approach largely based on the multi-component CFA records[12]. Down to 60 kyr BP a similar approach is used, largely controlled by the records with the highest resolution, i.e. visual stratigraphy, electrolytic conductivity and solid state direct voltage conductivity

(ECM)[13]. For even older ages, hence deeper ice, this age scale has been extended by a glaciological flow model. The timescale definition together with the thinning of annual layers due to glacier flow (Figure S4), which alters the achievable resolution of the record with depth, implies that the NH_4^+ information of a single year can be smeared out to the neighbouring years directly above and below in MIS3 and even more for older ages. To take this effect into account we also calculated a reduced outlier count, where we counted neighbouring outliers only as one. In this case the positive outlier count for n=3 was reduced to 3309, the negative outlier count to 518. This proves that neighbouring peaks occur quite often in the record, showing that the true resolution is often lower than 1 year for large parts of the record.

The outliers are not uniformly distributed over the entire record as illustrated in Figures 2-4. To quantify the temporal change in the biomass burning event frequency, we counted the number of identified outliers in a running window for the original and the reduced count, where a wider window width of 201 years was used to reduce the scatter in the FPF. We call this the original and reduced FPF. We did this both for positive and negative outliers. As the distribution of the logarithmic concentrations should be to first order symmetric around the median, the frequency of negative outliers in the 201 yr window allows us to correct the reduced FPF for counted positive peaks that are actually coming from the background distribution. We call this the corrected FPF. Note that while the original, reduced and corrected fire peak frequencies are obviously declining in absolute numbers, they show essentially the same temporal evolution during MIS3, implying that our conclusions on relative FPF changes do not depend on our corrections. For n=3 the corrected FPF ranges between 0 and 20 peaks per 201 yr window with systematically elevated peak counts during MIS3 interstadials (Figure S5).

Note that the FPF for the longest GI during MIS3, where background variability is slightly increased, is underestimated compared to neighbouring intervals, as the smallest fire events cannot be detected. Accordingly, the interstadial increase in FPF for those events would be even more pronounced if small fire events could be accounted for. The same holds true for the increase in FPF during the BA warming and after the YD event. The strongly increasing background variability for times prior to GS20 (together with the low resolution of the record in this deeper part of the ice core) does not allow us to count small fire events in this older part of the record. This is the main reason why no systematic changes in fire frequency can be found during those older interstadials. Accordingly, the FPF cannot be used in this time period to reliably quantify relative changes in fire recurrence.

As mentioned above the resolution to be achieved is dependent on the layer thickness at a given depth in the ice core, which does not suffice for truly annual resolution throughout the record. To check that our changes in the FPF are not just resolution effects, we performed several tests:

a) We tested that peaks identified in the high-resolution upper part of the record would also be detected after thinning and transforming them to MIS3 conditions. To this end, we used the record of the ice concentrations in the time interval from 10,275-11,275 yr BP and performed our peak detection with n=3. The ice concentrations were then transformed to recent atmospheric concentrations at the source (see below). This source concentration was then transformed into MIS3 ice concentrations using the typical accumulation and precipitation rates for a MIS3 stadial. This ice record was then smoothed by a running boxcar filter to reduce the resolution as expected from the ratio

of the layer thickness between the time window 10,000-11,000 years BP and a typical MIS3 stadial. Finally we performed the peak count with *n*=3 on this transformed record. As shown in Figure S6, 63 out of the 64 positive outliers in the original data were identified with our method after the data transformations. This shows that this running median/MAD method is able to accommodate the decline in resolution.

b) We used the annual data set of the atmospheric concentrations at the source and divided them into 6 bins of comparable layer thickness in the ice core, thus, keeping layer thickness relatively constant over a wide range of climate conditions (Figure S4). For each of these bins, we calculated the correlation between $\delta^{18}O$ as a proxy of temperature and peak count and plotted the result in Figure S7. Except for the bin with the smallest layer thickness (representative for the coldest parts in MIS4 and 5, where resolution is very low) and the bin with the largest layer thickness (representative of the late deglaciation, where resolution is not an issue) all layer thickness bins show a clear correlation between temperature and FPF for data younger than GI21. This indicates that there is a temperature effect on peak counts even if the layer thickness is kept within a very narrow band and supports our result that interstadials are connected to higher FPF during MIS3. Moreover, essentially the same linear relationship between peak count and temperatures holds for the entire range of layer thicknesses (Figure S7, bottom), again indicating that our variations in peak counts are not controlled by changes in the resolution of the record. When looking at data prior to GS20 (red dots in Figure S7, top), this correlation breaks down. As outlined above, this is mainly due to the increase in interannual variability in the NH_4^+ background concentrations in this older part of the record, which biases outlier detection to large peaks.

c) Finally, we also performed the analysis on the ice concentrations with a data set down-sampled to three-year averages, a resolution that can be clearly achieved throughout MIS3. Again we counted outliers in a 201 point (equivalent to 603 year) window with *n*=3. In this analysis (Figure S8), the FPF results from the annual data set for MIS3 are generally supported, although the resolution of the resolved variations is substantially lower. A notable exception is the lack of a peak in FPF in the center of DO event 8 (around 37,500 yr BP) for the triannual dataset. Looking at the triannual data itself it becomes apparent that there is actually not a lack in peaks during this time window, but instead that there are so many peaks that the running MAD is increased and becomes too large to detect the peaks in our outlier algorithm. Accordingly, this proves that this is not a resolution problem, but shows the limits of our peak detection method if the data set is too scattered. It should also be noted that due to the wide window, peaks in the FPF can change their exact position as a boxcar running window is not stable in terms of its phase relationship on timescales of the window width. For even older ages, the record would have to be down-sampled to 9-year averages, which is too long for a sensitive outlier detection. Moreover, the counting window would be 1800 years wide, which is wider than many of the DO events and phase relationships on DO event timescales cannot be resolved anymore. Accordingly, we cannot ascertain or falsify the results of our peak count prior to MIS3 by downsampling. It is however noteworthy that the overall variability in the data set as reflected in the MAD becomes larger in this old part of the record (Figure S3) and not smaller as expected from a degrading resolution.

The separation of background concentrations and fire peaks described above also allows us to quantify the typical NH_4^+ concentration of an identified fire peak in the ice core

record that exceeds the background concentrations. To this end we subtracted the background concentration (the running median in a 101 yr window) for a year, where a positive outlier has been detected, from the annual concentration of this respective year. This excess concentration is displayed in Figure S9 together with its 201 yr running median (the wider window is chosen to obtain a more stable estimate), providing a representative estimate of the typical source concentration for the events. As the background variability increases with warm climate conditions during MIS5 and during the last glacial/interglacial termination, only larger fire peaks can be separated from the background concentration during these warm intervals biasing the FPF to lower values. However, the lack of equally large excess fire concentrations during times of low background variability (MIS2-4) points to generally smaller fire events, potentially related to a reduced fuel availability, hence fire intensity, for those cold periods in parallel to the smaller vegetated surface area.

References

1 Bergin, M. H. *et al.* The contributions of snow, fog, and dry deposition to the summer flux of anions and cations at Summit, Greenland. *J Geophys Res* **100**, 16275-16288 (1995).

2 Davidson, C. I., Bergin, M. H. & Kuhns, H. D. in *Chemical exchange between the atmosphere and polar snow* Vol. 43 *NATO ASI Series* (eds E.W. Wolff & Bales R.C.) 275-306 (Springer Verlag, 1996).

3 Fischer, H., Wagenbach, D. & Kipfstuhl, J. Sulfate and nitrate firn concentrations on the Greenland ice sheet 1. Large-scale geographical deposition changes. *J Geophys Res* **103**, 21927-21934 (1998).

4 Kindler, P. *et al.* Temperature reconstruction from 10 to 120 kyr b2k from the NGRIP ice core. *Climate of the Past* **10**, 887–902, doi:10.5194/cp-10-887-2014 (2014).

5 Fischer, H., Siggaard-Andersen, M.-L., Ruth, U., Röthlisberger, R. & Wolff, E. Glacial/Interglacial changes in mineral dust and sea salt records in polar ice cores: sources, transport, deposition. *Rev Geophys* **45**, RG1002, doi:1010.1029/2005RG000192 (2007).

6 Dentener, F. J. & Crutzen, P. J. A Three-Dimensional Model of the Global Ammonia Cycle. *Journal of Atmospheric Chemistry* **19**, 331-369 (1994).

7 North Greenland Ice Core Project members. High resolution climate record of the northern hemisphere reaching into the last interglacial period. *Nature* **431**, 147-151, doi:10.1038/nature02805 (2004).
8 Sievering, H., Rusch, D. & Marquez, L. Nitric acid, particulate nitrate and ammonium in the continental free troposphere: nitrogen deosition to an alpine tundra ecosystem. *Atm Env* **30**, 2527-2537 (1996).
9 Ruth, U., Wagenbach, D., Steffensen, J. P. & Bigler, M. Continuous record of microparticle concentration and size distribution in the central Greenland NGRIP ice core during the last glacial period. *J Geophys Res* **108**, 4098, doi:4010.1029/2002JD002376 (2003).
10 Bloomfield, P. & Steiger, W. L. in *Least absolute deviations: Theory, applications and algorithms* 131-168 (Birkhaeuser, Boston, 1983).
11 Fischer, H., Wagenbach, D. & Kipfstuhl, J. Sulfate and nitrate firn concentrations on the Greenland ice sheet 2. Temporal anthropogenic deposition changes. *J Geophys Res* **103**, 21935-21942 (1998).
12 Rasmussen, S. O. *et al.* A new Greenland ice core chronology for the last glacial termination. *J Geophys Res* **111**, D06102, doi:06110.01029/02005JD006079 (2006).
13 Svensson, A. *et al.* A 60 000 year Greenland stratigraphic ice core chronology. *Climate of the Past* **4**, 47-57 (2008).
14 Fuhrer, K., Neftel, A., Anklin, M., Staffelbach, T., Legrand, M. High resolution ammonium ice core record covering a complete glacial-interglacial cycle. *J Geophys Res* **101**, 4147-4164 (1996).
15 Bigler, M. *Hochauflösende Spurenstoffmessungen an polaren Eisbohrkernen: Glazio-chemische und klimatische Prozessstudien* PhD thesis, University of Bern, (2004).
16 Sommer, S. *Hochauflösende Spurenstoffuntersuchungen an Eisbohrkernen aus Nord-Grönland* MSc thesis, University of Bern, (1996).
17 Bigler, M. *Entwicklung und Anwendung einer neuen Methode zur kontinuierlichen, hochaufgelösten Messung der Sulfatkonzentration an alpinen und polaren Eisbohrkernen* MSc thesis, University of Bern, (2000).
18 Gfeller, G. *et al.* Representativeness of major ions measurements and seasonality derived from NEEM firn cores. *The Cryosphere* **8**, 1855–1870, doi:10.5194/tc-8-1855-2014 (2014).
19 Sommer, S. *Klima-Informationen von chemischen Spurenstoffkonzentrationen in polaren Eisbohrkernen* PhD thesis, University of Bern, (2000).
20 Kaufmann, P. *et al.* An improved Continuous Flow Analysis (CFA) system for high-resolution field measurements on ice cores. *Environmental Science & Technology* **42**, 8044-8050, doi:10.1021/es8007722 (2008).

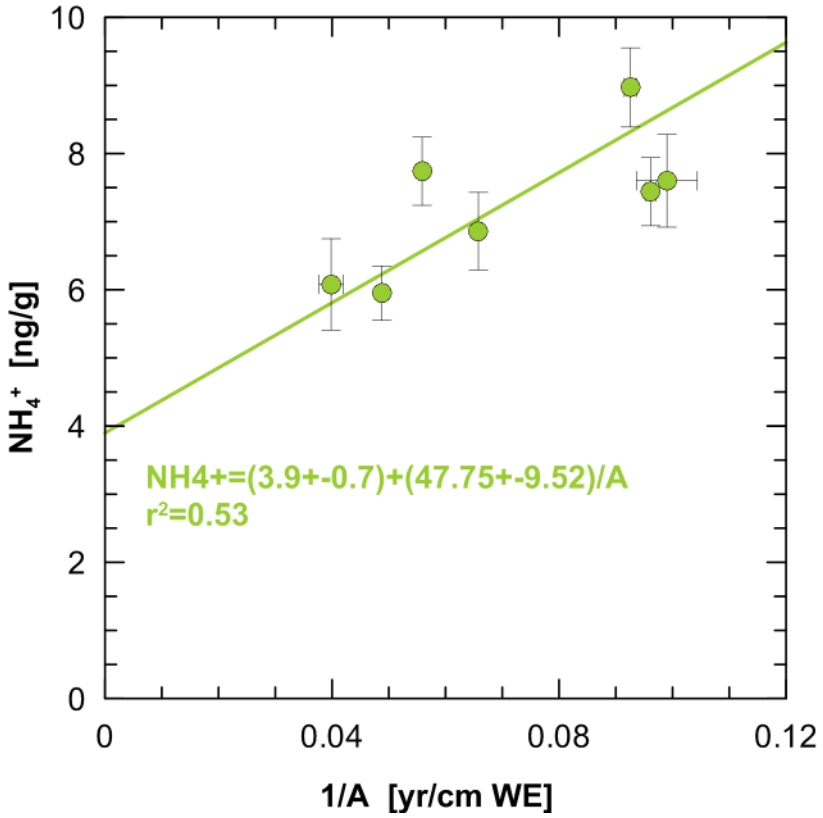

Figure S1: Spatial variations of NH_4^+ in Greenland ice – Displayed is the relation between NH_4^+ ice concentration and inverse snow accumulation at Central and Northern Greenland shallow ice cores sites (GRIP, B18, B20, B21, B26, B29, NEEM) over the last 2-5 centuries[14-19]. Error bars represent the standard error of the mean of all annual concentrations and accumulation values. The data points represent different time spans for the individual cores, however, as there is no significant trend in the data and since the accumulation values at each site are determined in the respective time span of each core, this does not cause a bias. The regression line is calculated using 2-sided linear regression. The uncertainty in the regression parameters is calculated by a Monte Carlo method, where the data points are varied within a Gaussian distribution with the standard deviation given by the error bars of each data point.

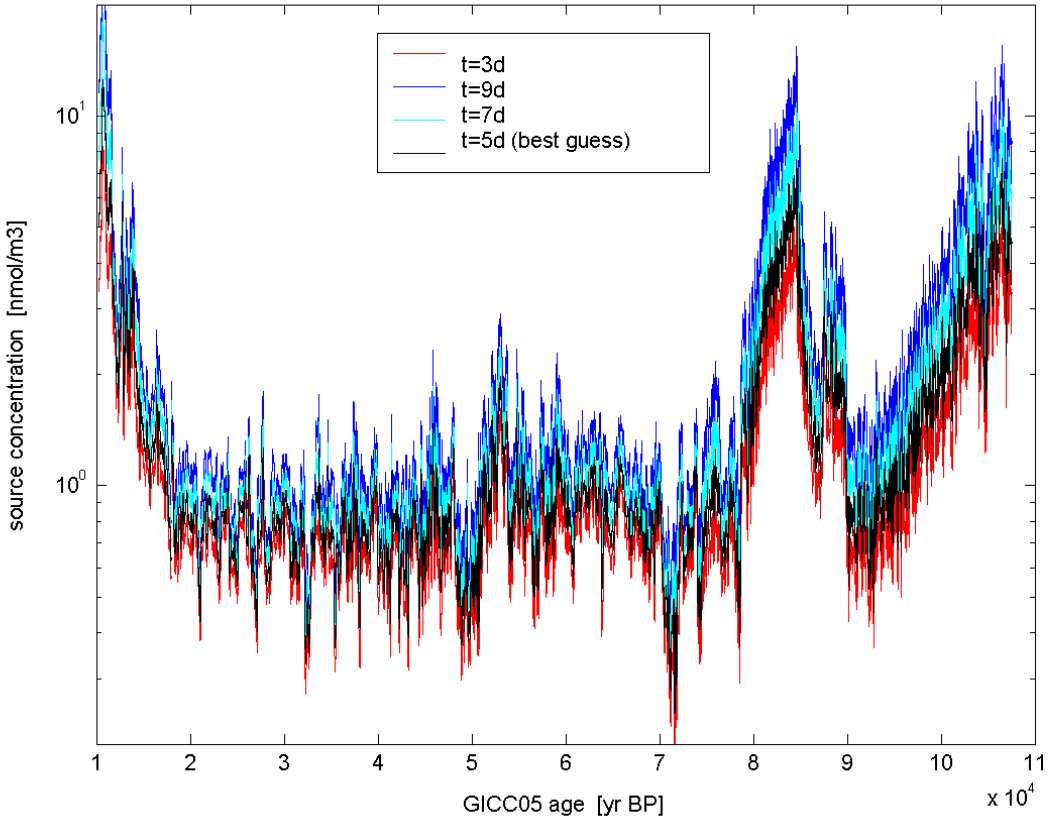

Figure S2: Effect of transport time on reconstructed aerosol concentration at the source – The different lines indicate the atmospheric aerosol concentration at the source reconstructed using transport times of t=3, 5, 7, and 9 days. For current conditions, back trajectories indicate a transport time of approximately 5 days for NH_4^+ aerosol from NA. As indicated in this figure, the spread in the four different reconstructions, can explain the stadial/interstadial range in NH_4^+ concentrations during MIS3, but not the larger glacial/interglacial changes.

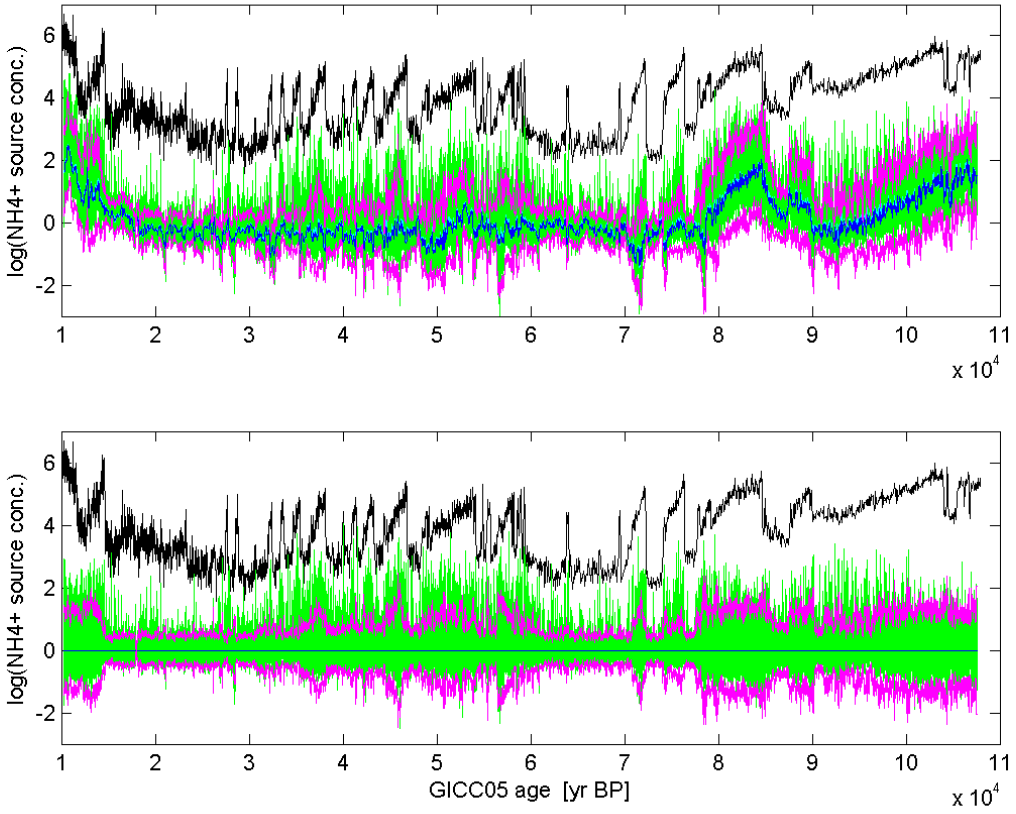

Figure S3: Variability in NH_4^+ annual concentrations – Top: running median (101 yr window) in the logarithmic annual concentration data at the source after removal of the peaks for *n*=3 (blue line) and including the peaks (light blue line, essentially hidden under the dark blue line). The magenta lines represent the median ± n times the MAD of the original annual data. All values of the annual data (green line) above the upper threshold are identified as biomass burning events. Bottom: the same as top but after subtracting the median values to better illustrate the variability varying with time. The black lines represent a re-scaled version of the NGRIP $\delta^{18}O$ record to visually illustrate cold and warm periods in the record.

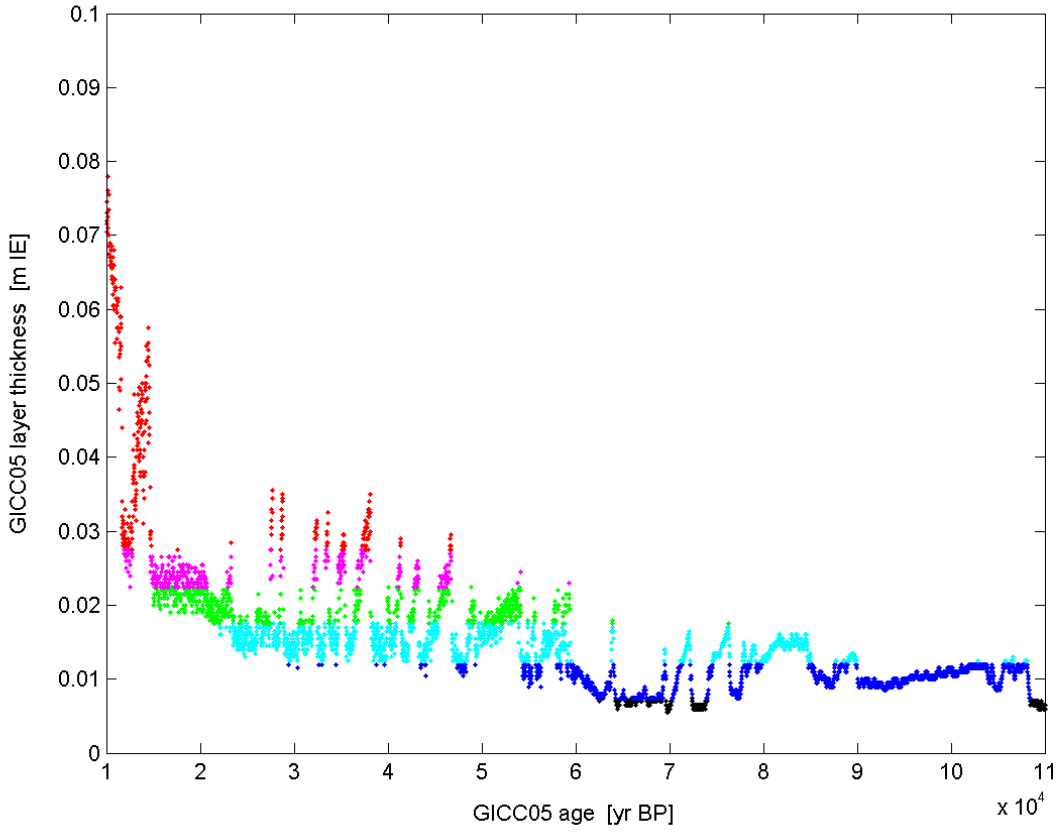

Figure S4: Layer thickness in m ice equivalent (IE) for the NGRIP ice core according to the model extended GICC05 age scale. Colors depict the bins of similar layer thickness used to test for the effect of resolution on the FPF as described in the text. The nominal resolution of the CFA NH_4^+ measurements is 1.2 cm[20], i.e. layers in dark blue and black, covering essentially MIS4 and 5, are thinner than the achievable resolution of the continuous flow analysis.

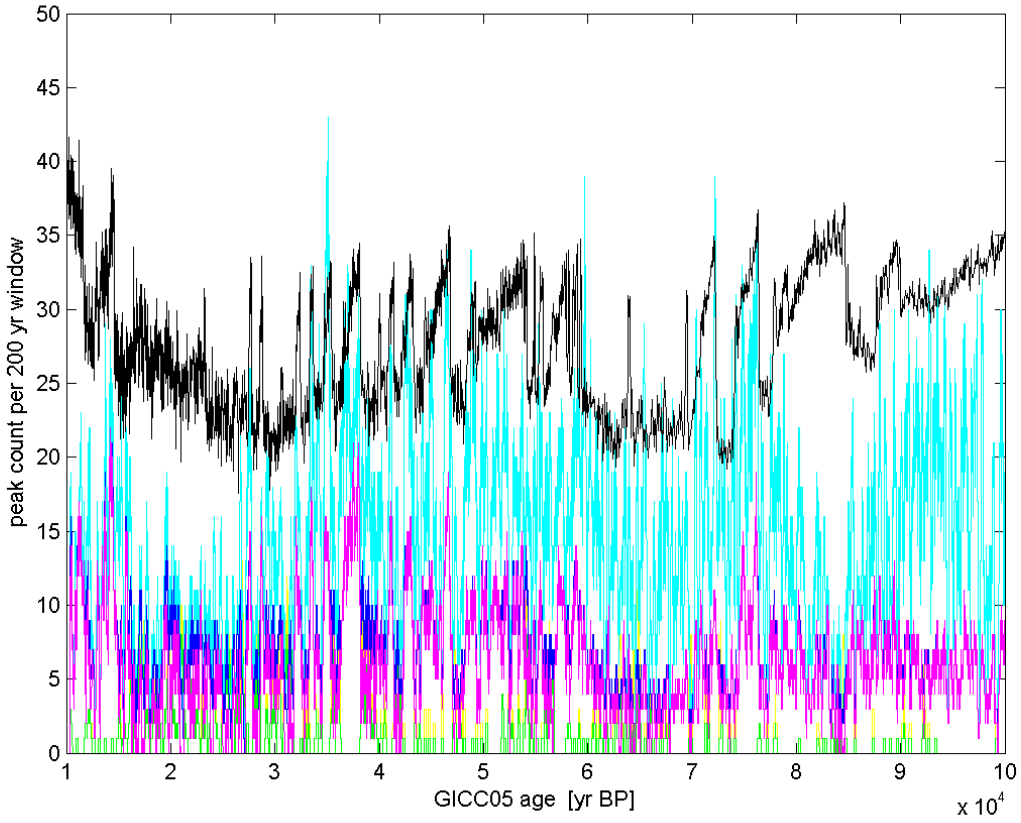

Figure S5: original (light blue line), reduced (dark blue line) and corrected count (purple line) of positive outliers in the logarithmic annual NH_4^+ concentrations at the source in a 201 year window, as detected above the threshold illustrated in Figure S3. Also displayed are the original (yellow line) and the reduced count (green line) of the negative outliers. The black line in the background provides a re-scaled version of the NGRIP $\delta^{18}O$ record to visually illustrate the occurrence of DO events.

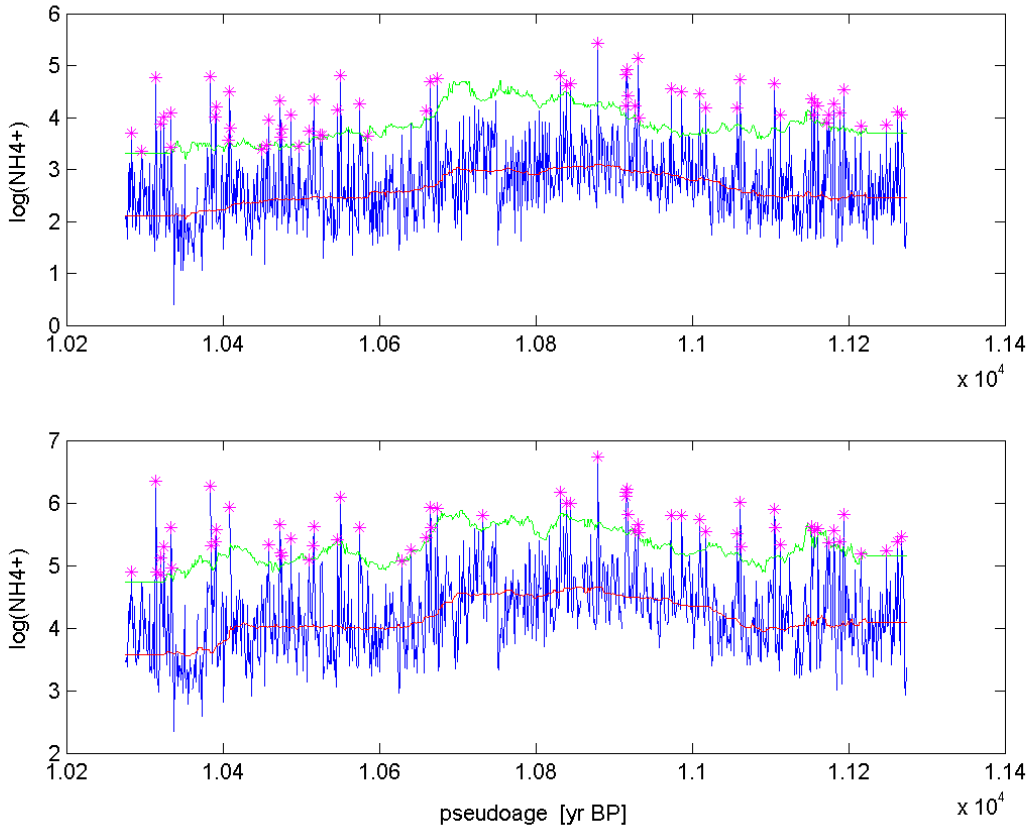

Figure S6: Test of peak count for reduced resolution – Top: Annual logarithmic NH_4^+ ice concentrations (blue line) in the time window 10,275-11,275, where the layer thickness is high enough to resolve seasonal cycles together with the running median (red line) + 3 times the MAD (green line) in a 101 yr window. All annual values above this threshold (purple stars) are detected as outliers. **Bottom:** Same as in the top but after transforming the annual concentrations to glacial deposition conditions and downsampling to adjust for the lower resolution as expected from the reduction in layer thickness from the late deglaciation (layer thickness 6.5 cm IE) to MIS 3 stadial conditions (layer thickness 1.2 cm IE).

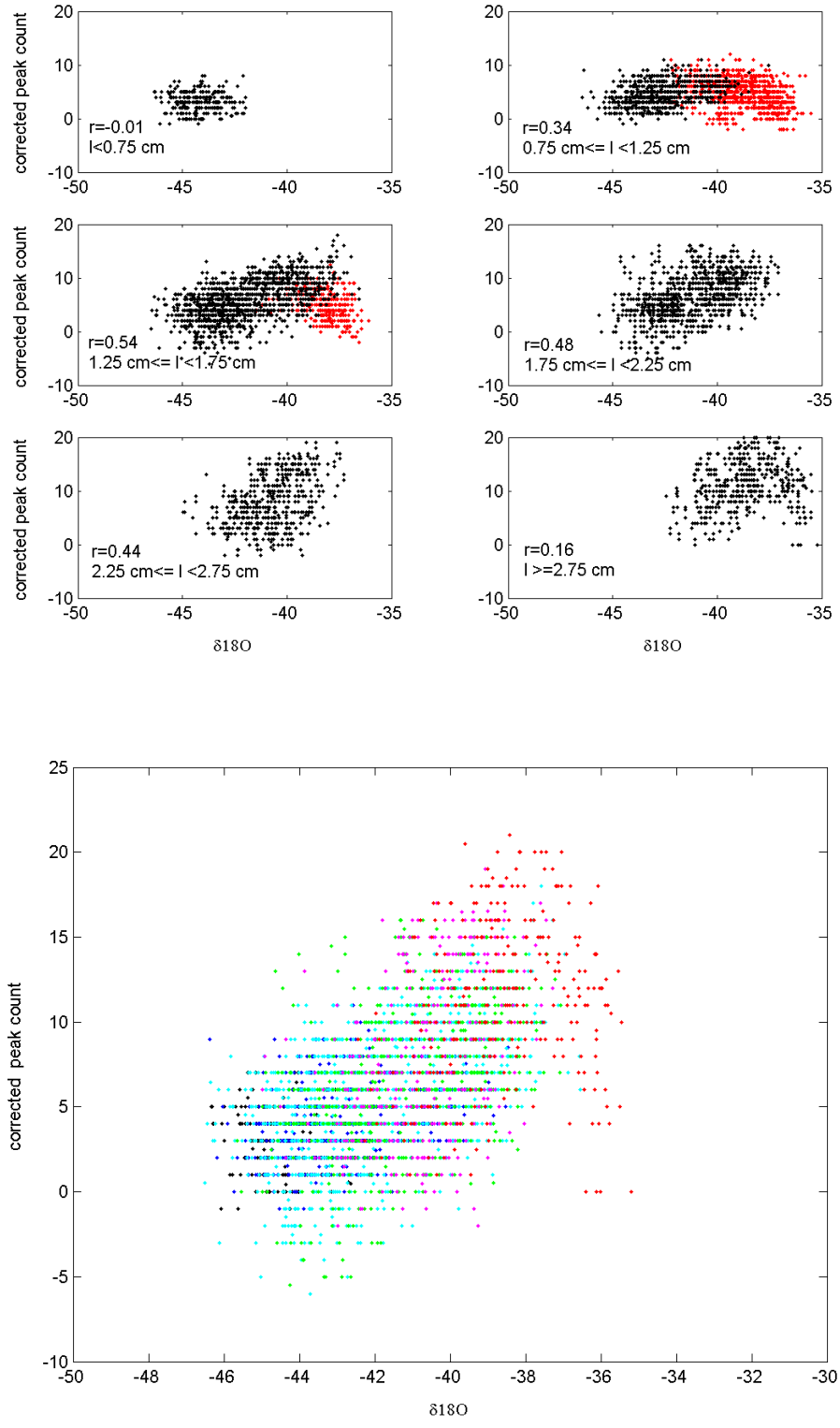

Figure S7: Resolution dependence of the FPF – Top 6 subpanels: each subplot shows the dependence of the corrected peak count on the NH_4^+ concentration at the source in a 201 year window with the temperature proxy $\delta^{18}O$ in a certain bin of layer thickness *l* as indicated in Figure S4. Black dots and correlation values refer to years younger than

80,000 years, red dots to years older than 80,000 years, where resolution is generally low. Bottom subpanel: Comparison of the linear relationship between corrected peak count and temperature for all 6 layer thickness bins for ages younger than 80,000 years, showing a similar temperature dependence over the entire range of layer thicknesses. Color coding is the same as in Figure S4.

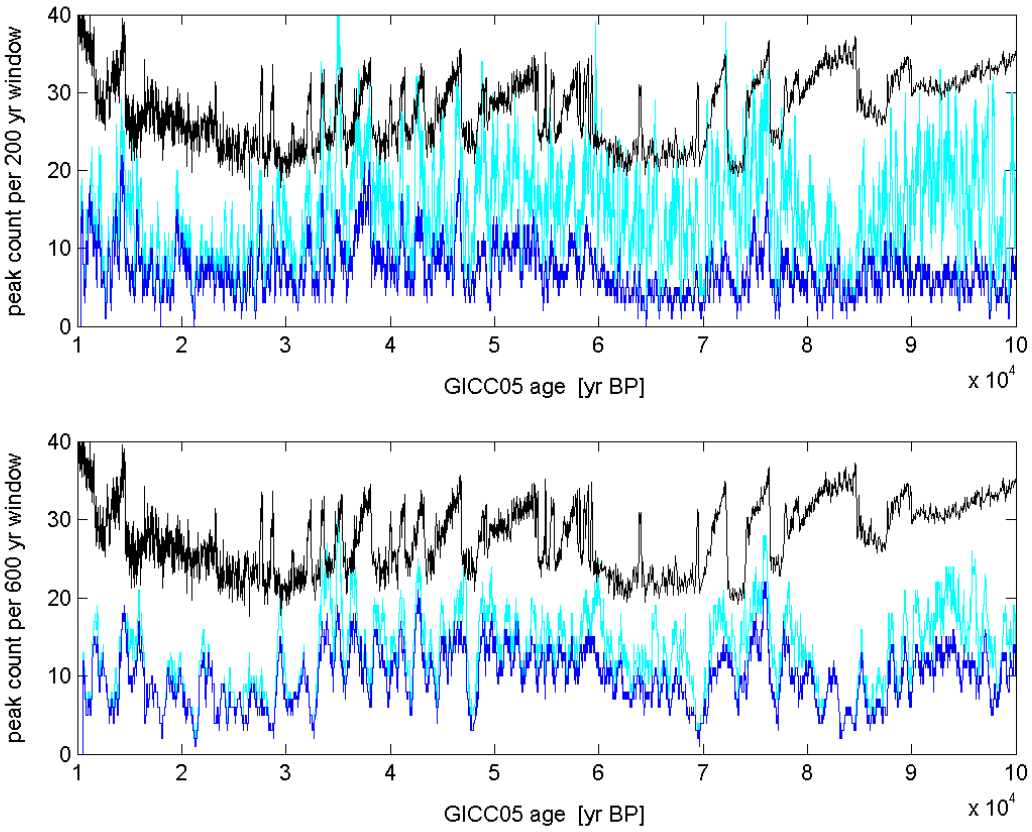

Figure S8: Comparison of different resolutions – Top: original (light blue line) and reduced count (dark blue line) of logarithmic annual NH_4^+ ice concentrations in a 201 yr window for *n*=3. **Bottom:** same as top but for 3-year averages. The black line provides a re-scaled version of the NGRIP $\delta^{18}O$ record to visually illustrate the occurrence of DO events. Note that the timing of narrow peaks is difficult to constrain in the bottom plot as the 600 yr wide running window can lead to phase changes on this timescale. A major difference on longer timescales between top and bottom is found in the interval 90-100,000 years BP, where the reduced count in the annual data is substantially lower than the original count, while in the 3 year data this is not the case, clearly illustrating oversampling in the annual data in this time window.

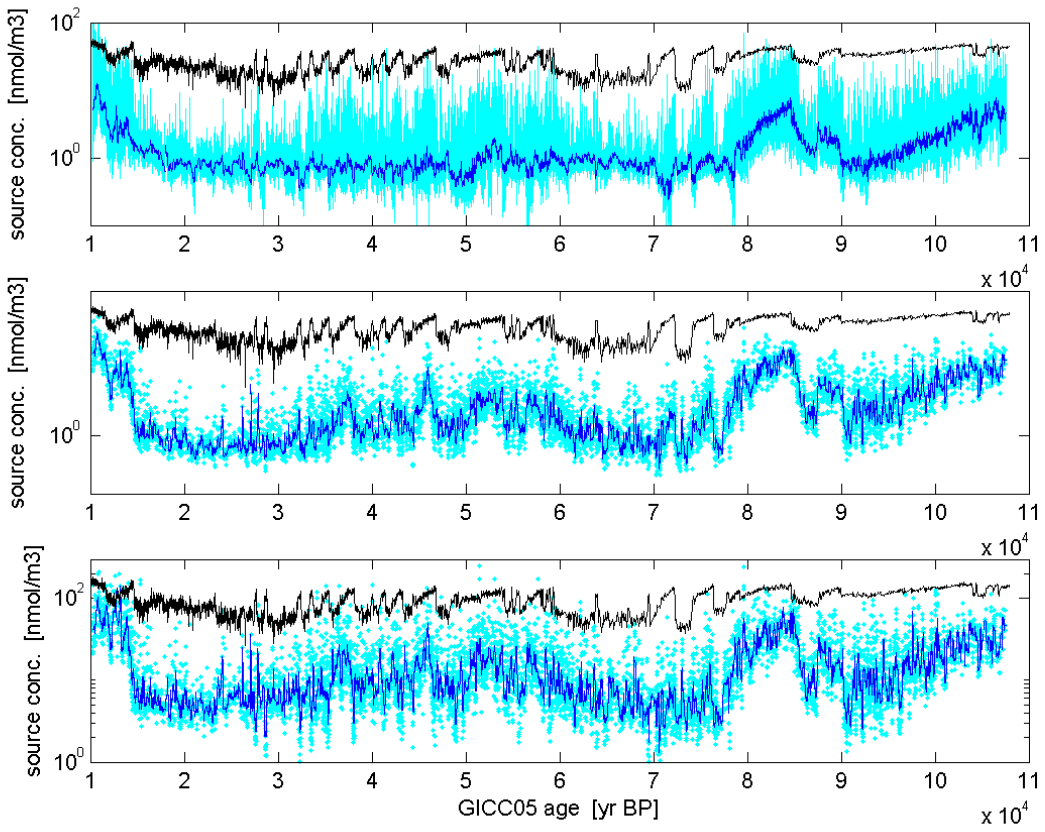

Figure S9: Comparison of background concentration and excess peak concentration at the source and in the ice – Top: The light blue line indicates the annual concentration at the source, the dark blue line its 101 year running median; Middle: the light blue dots show the concentration of detected positive outliers after subtracting the respective background concentration at the source, the dark blue line its 201 year running median. Bottom: same as middle but for ice concentrations. The black lines represent re-scaled versions of the NGRIP $\delta^{18}O$ record to visually indicate cold and warm periods.